Molecular Therapy
Original Article

Epitranscriptomics modifier pentostatin indirectly triggers Toll-like receptor 3 and can enhance immune infiltration in tumors

Marina Tusup,[1,3] Thomas M. Kündig,[1,2] and Steve Pascolo[1,2]

[1]University Hospital of Zürich, Department of Dermatology, Raemistrasse 100, 8091 Zürich, Switzerland; [2]Faculty of Medicine, University of Zurich, Zürich, Switzerland; [3]Faculty of Science, University of Zurich, Zürich, Switzerland

The adenosine deaminase inhibitor 2′-deoxycoformycin (pentostatin, Nipent) has been used since 1982 to treat leukemia and lymphoma, but its mode of action is still unknown. Pentostatin was reported to decrease methylation of cellular RNA. We discovered that RNA extracted from pentostatin-treated cells or mice has enhanced immunostimulating capacities. Accordingly, we demonstrated in mice that the anticancer activity of pentostatin required Toll-like receptor 3, the type I interferon receptor, and T cells. Upon systemic administration of pentostatin, type I interferon is produced locally in tumors, resulting in immune cell infiltration. We combined pentostatin with immune checkpoint inhibitors and observed synergistic anti-cancer activities. Our work identifies pentostatin as a new class of an anticancer immunostimulating drug that activates innate immunity within tumor tissues and synergizes with systemic T cell therapies.

INTRODUCTION

Among therapeutic antimetabolites, 2′-deoxycoformycin (pentostatin, Nipent) is an intriguing anti-cancer drug that has been used since the early 1980s to treat leukemia and lymphomas but has still an unknown mode of action. It is a natural adenosine analog produced by the bacterium *Streptomyces antibioticus* and the fungus *Emericella nidulans* and has been reported to be the most potent inhibitor of adenosine deaminase (ADA)[1]. However, pentostatin was found earlier to have no toxicity toward tumor cells *in vitro*[2,3] (lymphoid and non-lymphoid origins) even at high concentrations (Figure S1). It was also reported to be ineffective as a monotherapy in several mouse tumor models.[4] Nevertheless, because lymphocytes are particularly dependent on ADA activity, pentostatin was tested in cancer patients and found to be efficacious against several hematologic malignancies (chronic lymphocytic leukemia;[5] prolymphocytic leukemia;[6] Hodgkin lymphoma;[7] adult T cell lymphoma-leukemia, especially cutaneous T cell lymphomas;[8,9] and low-grade non-Hodgkin's lymphomas),[10] particularly against hairy-cell leukemia.[11,12] Therefore, it replaced systemic administration of recombinant interferon alpha-2a (IFN-α-2a), which was the only treatment before pentostatin found to be efficacious against this type of leukemic malignancy.[13] Although the mechanism of pentostatin's anti-cancer efficacy is still unknown 35 years after its introduction into clinical practice, the drug was reported to induce clear systemic biochemical changes: inhibition of ADA impedes conversion of adenosine into inosine and thereby induces (deoxy)adenosine accumulation. High deoxy-ATP can cause an accumulation of DNA strand breaks in cells, but this did not play a role in the antitumor activity of pentostatin.[14] A high (deoxy)adenosine concentration also hinders S-adenosyl-L-homocysteine (SAH) hydrolase activity, leading to an increase in SAH, which is a potent inhibitor of S-adenosylmethionine (SAM)-involving reactions. The decreased SAM to SAH ratio (known as the methylation index)[15–17] leads to lower methylation in cellular RNA.[18] Indeed, cells from pentostatin-treated patients showed a 10-fold reduction in the methylation index and a strong decrease in 2′O-methylation of cellular RNA lasting a few days after injection of the drug.[18] Methylation in RNA is well established to prevent this endogenous molecule from triggering immune receptors of the Toll-like receptor (TLR)[19] and retinoic acid-inducible gene I (RIG-I)-like receptor (RLR) families[20,21] (a recent review was reported by Freund et al.[22]). Thus, we investigated the immunostimulating capacities of RNA extracted from pentostatin-treated cells or organs from pentostatin-injected mice.

RESULTS AND DISCUSSION

Total RNA extracted from cells or organs was mixed with protamine to generate nanoparticles (Figure S2A).[23,24] These particles trigger the production of inflammatory cytokines such as tumor necrosis factor alpha (TNF-α) in human peripheral blood mononuclear cells (hPBMCs) independent of the RNA origin (Figure S2B). Of note, liposomal formulations of human cellular RNA do not stimulate such TNF-α production in hPBMCs, as previously reported[19] (Figure S2C). Meanwhile, protamine-RNA nanoparticles strongly induce type I IFN in hPBMCs only when cellular RNA originates from lower organisms pointing to biochemical differences in the composition of RNA from different species as previously reported[19] (Figure S2D). The protamine-RNA nanoparticles trigger higher

Received 14 May 2021; accepted 20 September 2021;
https://doi.org/10.1016/j.ymthe.2021.09.022.

Correspondence: Steve Pascolo, University Hospital of Zürich, Department of Dermatology, Raemistrasse 100, 8091 Zürich, Switzerland.
E-mail: steve.pascolo@usz.ch

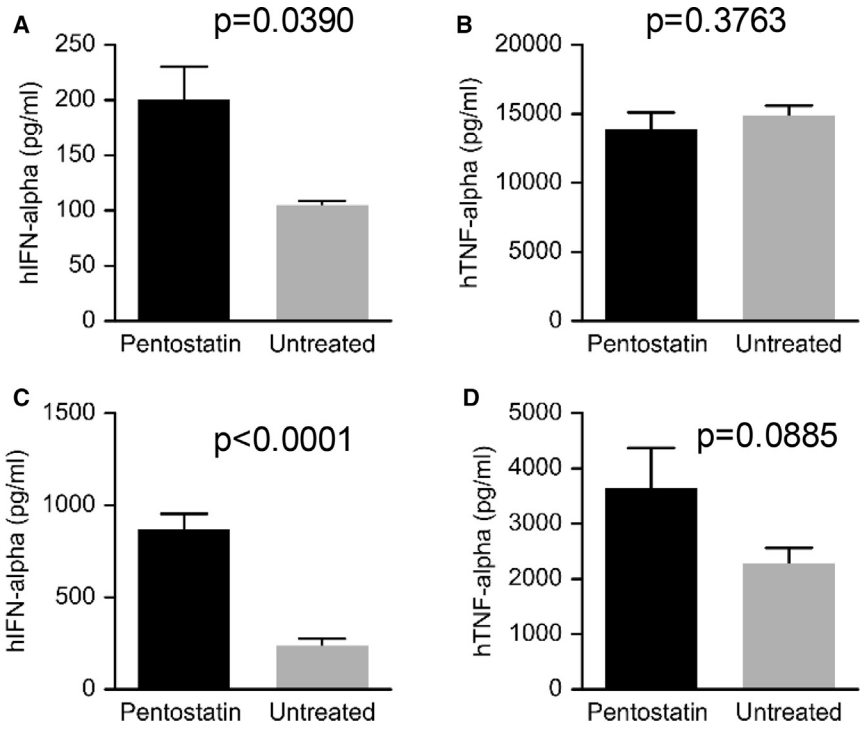

Figure 1. Pentostatin enhances the potential of total RNA from cells or organs to induce human interferon alpha (hIFN-α) in hPBMCs incubated with protamine-RNA nanoparticles

Total RNA was extracted from HEK cells (A and B) that were untreated or treated with 0.3 μg/mL (equivalent to clinical dose) of pentostatin for 72 h and then formulated with protamine to generate nanoparticles, which were incubated overnight with hPBMCs. hIFN-α and human TNF alpha (hTNF-α) concentrations in supernatants were quantified by ELISA. Experimental duplicates. Error bars, mean ± SD. The p value obtained by a t test is indicated. (C and D). Total RNA extracted from mouse kidneys collected 18 h after mice was intravenously injected with 10 μg of pentostatin or from untreated mice was combined with protamine to generate protamine-RNA nanoparticles, which were incubated with hPBMCs overnight. hIFN-α and hTNF-α concentrations in supernatants were quantified by ELISA. Biological duplicates with experimental duplicates and the technical duplicate of each. Error bars, mean ± SD. The p values obtained by a t test are indicated.

type I IFN when both single-stranded (ss)RNA and double-stranded (ds)RNA are condensed together, and TLR3 is present (Figure S2E), indicating that these particles can synergistically engage TLR7 and TLR3 when both ligands are co-packaged. Total RNA extracted from tumor cells treated *in vitro* with pentostatin had higher type I IFN induction capacities in hPBMCs than RNA extracted from untreated cells (Figure 1A for RNA from human HEK cells and Figure S3A for RNA from mouse CT26 cells). The TNF-α induction capacity of RNA was not significantly affected by pentostatin treatment (Figure 1B). Similarly, RNA extracted from the organs of mice injected intravenously with pentostatin induced more IFN-α production in hPBMCs than RNA extracted from the organs of untreated mice (Figures 1C and 1D for RNA from kidneys and Figures S3B and S3C with RNA from tumors and spleens, respectively). Meanwhile, pentostatin alone is not directly immunostimulating (Figures S3D and S3E on mouse splenocytes and hPBMCs, respectively). These data prompted us to investigate whether the anti-cancer effects of pentostatin are mediated by the immune system. Indeed, we found that the drug exhibited anti-cancer activity only in mouse tumor models in which immune checkpoint inhibitors (reviewed in Grosso and Jure-Kunkel[25]) were also efficacious: MB49 tumors in C57BL/6 mice and CT26 tumors in BALB/c mice (Figure S4). Immune mediators were required to induce anti-tumor responses after pentostatin intravenous injection: type I IFN receptor (IFNAR) (Figure 2A) and T cells (Figure 2B). Mice cured by pentostatin were protected from a tumor challenge (Figure 2C). Histological studies indicated that after pentostatin injection, tumors were infiltrated with T cells (Figure 2D). Thus, pentostatin can enhance immune infiltration in tumors. Heterozygous reporter mice carrying luciferase reporter genes under the control of an IFN beta (IFN-β) promoter[26] were used to monitor IFN-β induction in tumor-bearing mice. After pentostatin injection, a luciferase signal was detected in the tumor (Figure 2E). The local induction of type I IFN in tumors and the requirement for the type I IFN receptor for pentostatin activity are particularly striking since before pentostatin was introduced in 1984, hairy cell leukemia was treated with recombinant IFN-α-2a. To further investigate the link between RNA sensing and pentostatin, we tested the efficacy of the drug in TLR3, TLR7, and mitochondrial antiviral-signaling protein (MAVS, deficient signal transduction from RIG-I and melanoma differentiation-associated protein 5 (MDA-5))-knockout (KO) mice. The efficacy of pentostatin was decreased only in the TLR3-KO mice (Figures 3 and S5A). Accordingly, TIR-domain-containing adapter-inducing interferon-β (TRIF)-KO mice also did not respond to the drug treatment (Figure S5B). MAVS deletion had no effect on pentostatin efficacy, showing that the RIG-I and MDA-5 cytoplasmic receptors are not involved in the type I IFN response induced after injection of the ADA inhibitor. Apart from the known demethylation of cellular RNA, induction of new dsRNA by pentostatin may be responsible for triggering TLR3. Thus, we evaluated total dsRNA content, the expression of endogenous retroviruses, and A-to-G editing by adenosine deaminases acting on RNA (ADAR) (this activity lowers the presence of long-paired RNA stretches). As presented in Figure S6, none of these parameters is affected by pentostatin. Thus, our experiments demonstrated that pentostatin, which is known to decrease methylation of cellular RNA, triggers TLR3 in pathological tissues (e.g., due to the release of cellular RNA by necrosis) and activates type I IFN production (probably by $CD141^+$ conventional dendritic cells that have been

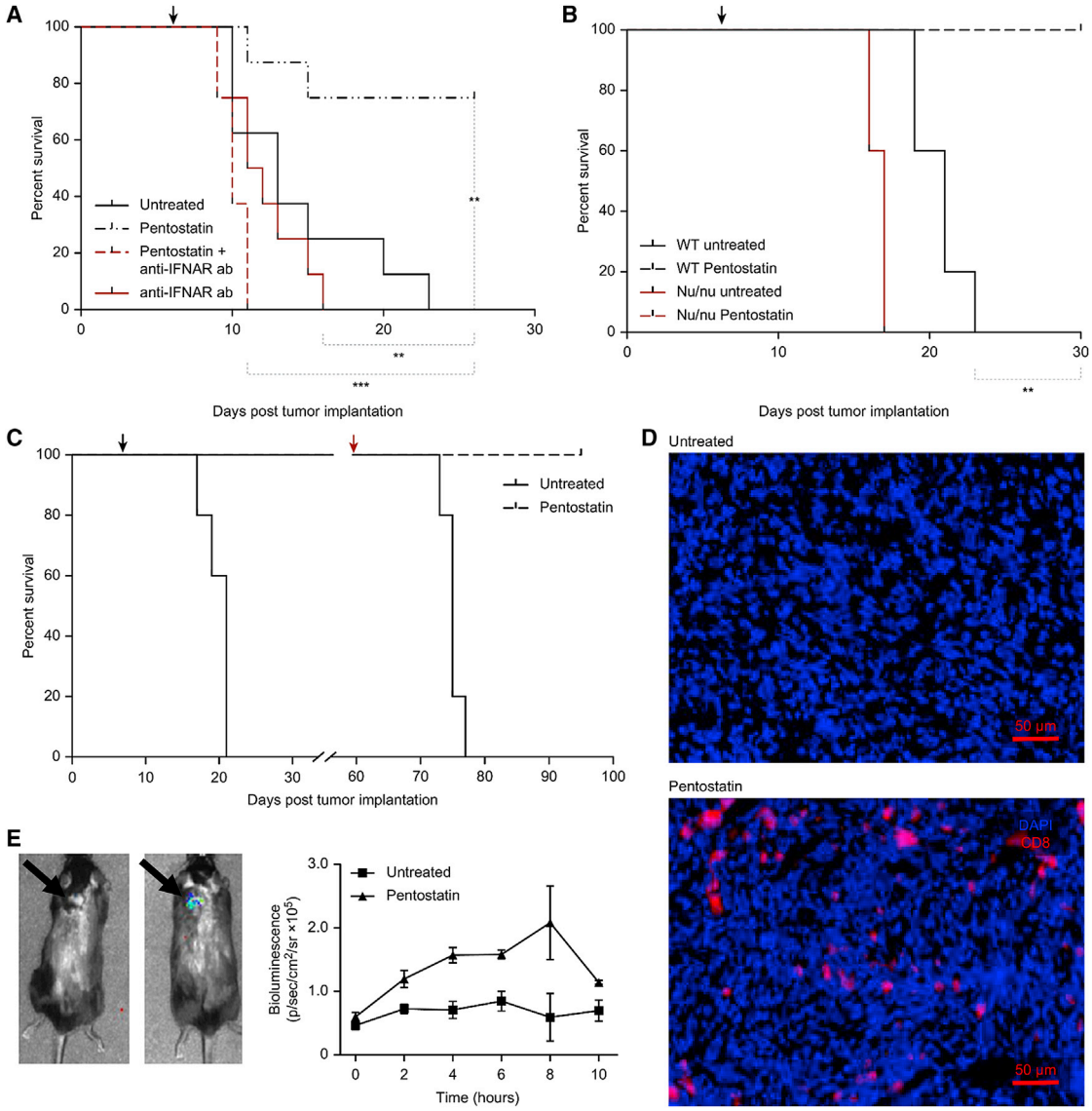

Figure 2. Pentostatin activity *in vivo* in tumor-bearing mice requires type I IFN and T cells

(A) Mice were implanted subcutaneously with CT26/NY-ESO-1 cells and received 10 µg of intravenous pentostatin alone ("Pentostatin") or together with 1 mg intraperitoneally of an anti-IFNAR antibody ("Pentostatin + anti-IFNAR ab") 6 days later. As controls, tumor-bearing mice received only the anti-IFNAR ab ("anti-IFNAR ab") or were left untreated ("Untreated") at day 6. The results show that pentostatin can be used to treat CT26/NY-ESO-1 tumors, but its activity is abrogated by anti-IFNAR ab; n = 8 in each group. The black arrow points to the day of pentostatin treatment. The significance of differences between the survival curves was calculated with the log-rank (Mantel-Cox) test. ***p = 0.0007 for pentostatin versus pentostatin + anti-IFNAR ab; **p = 0.0025 for pentostatin versus untreated; **p = 0.0014 for pentostatin versus anti-IFNAR ab. (B) The survival of CT26/NY-ESO-1 tumor-bearing nude (Nu\nu) and wild-type (WT) mice treated with pentostatin on day 6 (10 µg intravenously) and untreated mice was assessed. T cell-deficient Nu/nu mice showed no response to pentostatin treatment (survival was identical in pentostatin and untreated groups); n = 5 in each group. The black arrow points to the day of pentostatin treatment. The significance of differences between the survival curves for WT-untreated mice versus pentostatin-treated mice was calculated with the log-rank (Mantel-Cox) test. **p = 0.0019. (C) CT26/NY-ESO-1 tumor-bearing mice treated and cured with pentostatin (10 µg intravenously, black arrow) were re-challenged (red arrow) with the same tumor cells at day 60 after initial tumor implantation. For more than 90 days, they showed no tumor growth. In parallel, an untreated group was implanted with tumors and showed expected tumor progression and death (n = 5). (D) Immunofluorescent staining of cryo-sections created from established CT26/NY-ESO-1 tumors taken from mice 36 h after pentostatin treatment or from untreated mice shows that pentostatin treatment results in infiltration of T lymphocytes. Numerous $CD8^+$ cells can be detected only in tumors from pentostatin-treated mice. DAPI staining for nucleated cells; PE-Texas red staining of $CD8^+$ cells; 20× magnification. (E) We measured bioluminescence *in vivo* in day-6 MB49 tumor-bearing heterozygous reporter IFN-$\beta^+/\Delta\beta$-luc B6 mice (kindly provided by Dr. Stefan Lienenklaus from Hannover, Germany) injected with pentostatin (the mouse on the right) or untreated mice (the mouse on the left). 6 h after intravenous injection of pentostatin, luciferin was administered intraperitoneally, and anesthetized mice were imaged using the *in vivo* imaging system (IVIS Lumina instrument [PerkinElmer], binning 8, exposure time 3 min). At the tumor site (indicated by the black arrow), only mice having received pentostatin showed luciferase expression. The graph presents the quantification of the signal at the tumor site in treated and untreated mice over 10 h, 2 mice per group (2-way ANOVA, p = 0.0141).

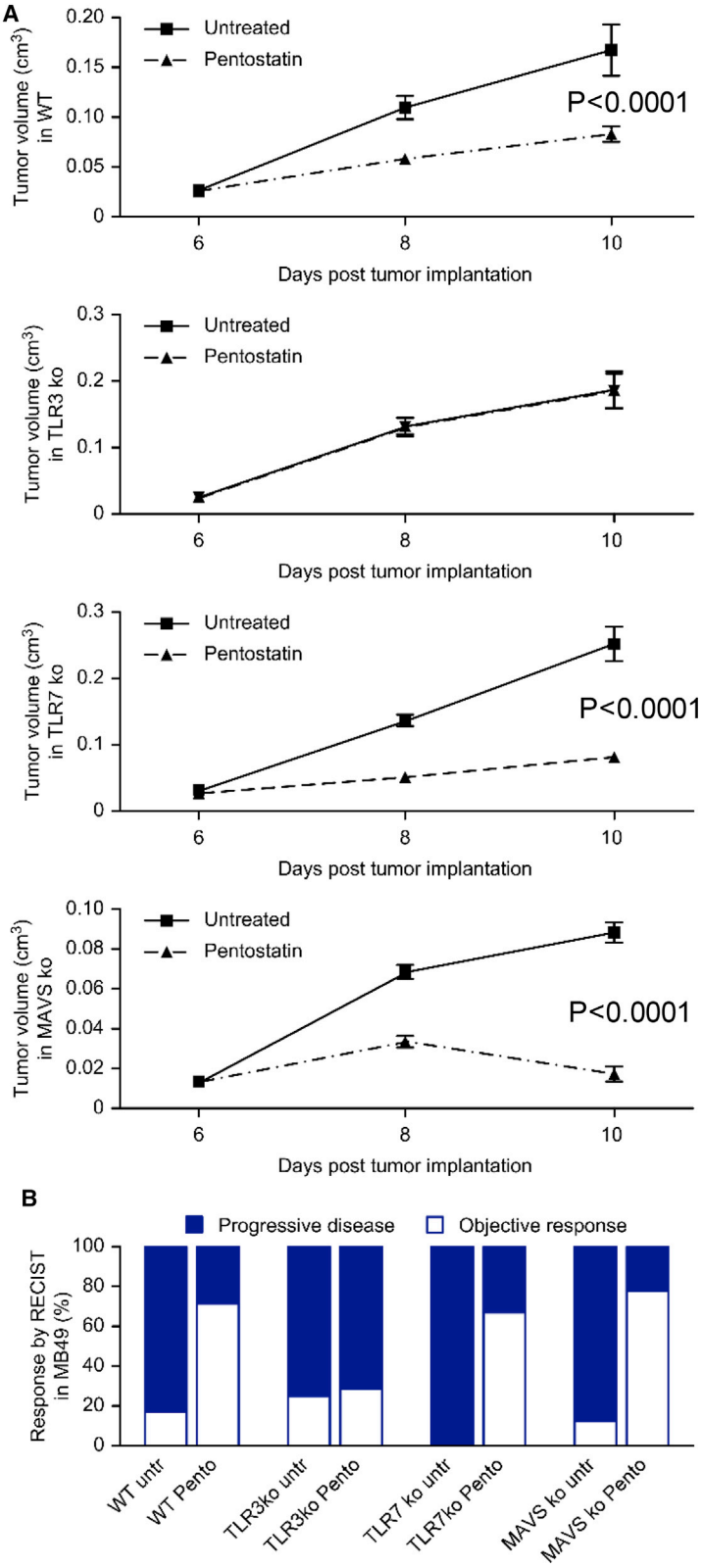

Figure 3. Pentostatin anti-cancer activity *in vivo* requires TLR3

MB49 tumor cells were implanted subcutaneously in WT, TLR3-KO, TLR7-KO, or MAVS-KO mice. A day-6, 10 μg of pentostatin was administered intravenously in some mice, whereas a control group was left untreated. Tumor volumes were measured every other day using a caliper and the following formula: (largest diameter × perpendicular diameter^2/2). The data in (A) show that pentostatin could control tumor growth in all groups except for the TLR3-KO mice. Error bars, mean ± SEM. p values obtained by 2-way ANOVA are indicated. (B) The responsiveness of MB49 tumor-bearing mice is summarized in stacked bars according to the response evaluation criteria in solid tumors (RECIST) criteria adapted to mice and accounting for tumor size at day 6 versus day 10. Progressive disease is defined as at least a 20% increase in tumor volume, whereas an objective response is defined as stable disease (less than a 20% increase) or a decrease in tumor volume. The following includes number of mice per group: WT n = 7, TLR3-KO n = 7, TLR7-KO n = 6, and MAVS-KO n = 7. More objective responses can be observed in pentostatin-treated versus untreated mice among the WT, TLR7-KO, and MAVS-KO mice, whereas in TLR3-KO mice, no difference was identified between untreated and pentostatin-injected mice.

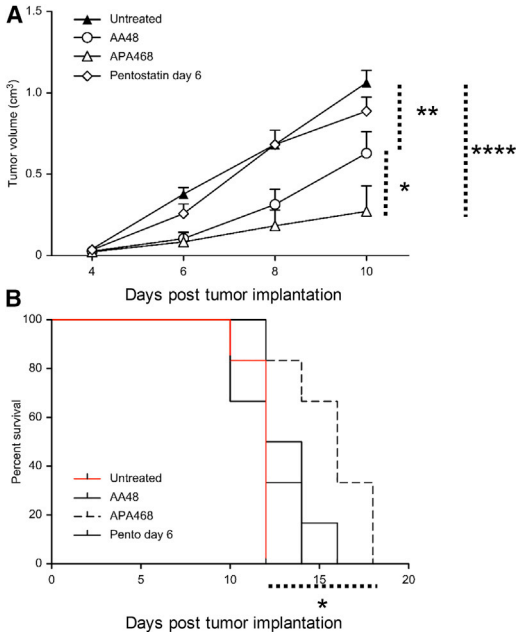

Figure 4. Pentostatin converts inefficient therapy with immune checkpoint inhibitors into efficient therapy

B16 tumor cells were implanted subcutaneously in WT C57BL/6 mice. Three groups of 6 mice each received the following treatments: anti-PD1 antibody (100 μg per mouse intravenously) at day 4 and day 8 (AA48), pentostatin (10 μg per mouse intravenously) at day 6 (Pento day 6), anti-PD1 antibody (100 μg per mouse intravenously) at day 4 and day 8, and pentostatin (10 μg per mouse intravenously) at day 6 (APA468). The graph in (A) shows the tumor sizes over time. Both anti-PD1 and anti-PD1 with pentostatin gave significant delay in tumor growth compared to untreated (two-way ANOVA; p values are 0.0054 and <0.0001, respectively), whereas pentostatin alone had no effect (two-way ANOVA; p value is 0.1758). Importantly, the combination of anti-PD1 and pentostatin was significantly better than anti-PD1 alone (two-way ANOVA; p value is 0.0464). The survival of mice shown in (B) also indicates that only the combination of the two drugs could lead to significant efficacy of the anti-cancer treatment (Mantel-Cox SPSS; calculation to compare three or more groups, p = 0.0081).

found to give the greatest production of IFN-α upon synthetic dsRNA exposure[27]) in tumors, allowing infiltration of immune cells and thus controlling tumor growth. One limit of immunotherapy using immune checkpoint inhibitors is that activated cells do not penetrate "cold tumors." Knowing that type I IFN controls infiltration of T cells[28] and that it is induced in tumors by pentostatin, we rationalized combining pentostatin with anti-programmed cell death protein 1 (PD1) antibodies in a B16 melanoma model, where both reagents were not very efficacious when used individually. This combination elicited a tumor response that is stronger than the one observed with each drug alone (Figure 4A) and is the only one that extended overall survival (Figure 4B).

Our experiments show that the anti-cancer drug pentostatin, which is known to be not directly toxic to tumor cells but lowers the methylation index and thereby methylation of cellular RNA, actually triggers TLR3-TRIF signaling in tumors to induce local production of type I IFN. Thus, pentostatin, which is classified as a chemotherapy drug, should be reclassified as an original immunotherapeutic drug. Its capacity to enhance immune infiltration in tumors allows better control of cancers. Pentostatin synergizes with anti-PD1 therapy. Discovery of the original mode of action of pentostatin will allow repurposing of this drug for combination treatments incorporating local induction of type I IFN at tumor sites with T cell therapies, including immune checkpoint inhibitors, chimeric antigen receptor (CAR)-T cells, or reprogrammed T cells. In addition, the mode of action of pentostatin could make it relevant as an anti-viral therapy, particularly against RNA viruses. Indeed, by demasking the genome of such viruses, it would stimulate production of the anti-virus type I IFNs. Thus, we expect that pentostatin will become an important drug in future immunological treatments for cancer and eventually for infectious diseases.

MATERIALS AND METHODS

Mice

Wild-type (WT) and nude mice were purchased from Envigo. Tlr3$^{-/-}$, Tlr7$^{-/-}$, MAVS$^{-/-}$, and TRIF$^{-/-}$ (all have C57BL/6 genetic background) were bred in-house. IFN-β/Luc reporter mice were kindly provided by Dr. Stefan Lienenklaus (University of Hannover, Germany) and bred in-house.

Age-matched (6–12 weeks) female and male animals were used throughout experiments. Animal experiments were approved by the regulatory authorities (license 175/2015, "Study of the immunological anti-cancer effects of pentostatin, an ADA inhibitor"). All mice were kept in accordance with regulations from the Laboratory Animal Services Center (LASC) at the University Hospital of Zurich.

Tumor cell lines

CT26/NY-ESO-1 is a murine colorectal cancer cell line expressing NY-ESO-1 and was kindly provided by Professor Hiroyoshi Nishikawa.[29] The MB49 bladder cancer cell line was kindly provided by Dr. Sonia Domingos-Pereira (University Hospital of Lausanne, Switzerland). B16F10 and EL4 were available in our laboratory. All cell lines were kept in "RPMI" medium (Gibco) containing 10% fetal bovine serum (Thermo Fisher Scientific), 100 μg/mL Normocin, and 2 mM L-glutamine ("complete medium"). Cells were tested for pathogens and approved from the LASC regulatory office. In-house testing for mycoplasma was performed routinely.

RNAs

E. coli, human muscle, human pancreas, and HeLa RNAs were ordered from Ambion (Thermo Fisher Scientific). Total RNA from cells or tissues or flies (*D. melanogaster* flies provided by Julia Falschlunger, University of Zurich, Switzerland) was obtained using the miRNeasy Mini Kit (QIAGEN) according to the manufacturer's instructions. For the isolation of RNA from yeast, tablets of dormant *S. cerevisiae* were reactivated in water solution containing 1% D-glucose and 0.1% yeast extract kept at 28°−30° with slow steering for 6−8 h before a mixture of lyticase/zymolase was employed in combination with "RLT" (QIAGEN) buffer to lyse cells. All RNAs

were checked either on 1.2% agarose containing 1% 3-(N-Morpholino)propane sulfonic acid (MOPS)-EDTA and 0.75% of 37% formaldehyde (Sigma) or on Agilent RNA 600 Nano chips using the 2100 Agilent bioanalyzer. Agilent bioanalyzer and software were kindly provided by Silvia Lang (University Hospital Zurich, Switzerland).

Protamine-RNA formulations

Protamine (from IPEX) was purchased from Meda and stored at 4°C. Total RNA diluted in water at 0.5 mg/mL was combined with protamine diluted in water at 0.5 mg/mL as described.[23,24] 1 μg of diluted total RNA mixed with 2 μg of diluted protamine was incubated at room temperature (RT) for 10 min before addition of 200 μL of complete medium containing one million hPBMCs and incubation 24 h at 37°C in a CO_2 incubator.

ELISAs

Human (h)IFN-α pan (Mabtech) and TNF-α (BioLegend) were measured in fresh and frozen cell-culture supernatants following the manufacturer's protocols.

For the measurement of dsRNA, the anti-dsRNA antibody J2 (a purified mouse immunoglobulin [Ig]G-2a obtained from Scicons) was coated overnight at 1 μg/mL, and the wells were saturated for 1 h with ELISA buffer (eBioscience). Total RNA was diluted at 10 μg/mL in cold ELISA buffer and incubated for 1 h in the ELISA system. After washes, the anti-dsRNA antibody K2 (an unpurified mouse IgM obtained from Scicons) was added in wells (the cell supernatant containing the antibody was diluted in 8 vol of ELISA buffer) and incubated for 1 h before washes. Then, a detection antibody, goat anti-mouse IgM polyclonal horseradish peroxidase (HRP)-conjugated antibody (Abcam), was used to detect mouse IgM. All of those incubations were performed at 4°C to protect RNA from degradation. After washes, TMB buffer was added, and the reaction was stopped by sulfuric acid. A titration of poly(I:C) was used as a standard. Optical densities (ODs) were read on a BioTek Instruments reader at 450 nm using Gen5 software.

VeriPlex human cytokine 16-Plex ELISA (PBL) was employed for multiple cytokine measurements according to the manufacturer's protocol. ImageJ was used as a software for quantifying values obtained from chemiluminescent measurement of VeriPlex ELISA.

Real-time PCR

HEK cells were cultured for 2 days in the presence of 0, 7.5, 15, or 30 μg/mL pentostatin. Total RNA was extracted with miRNeasy (QIAGEN), and 1 μg was reverse transcribed using the High-Capacity cDNA Reverse Transcription Kit from Applied Biosystems as recommended by the manufacturer. An equivalent of 16 ng of initial RNA was used per well in real-time PCR (BRYT Green Dye, GoTaq; Promega) using primers specific for housekeeping genes (glyceraldehyde-3-phosphate dehydrogenase [GAPDH] and hypoxanthine-guanine phosphoribosyltransferase [HPRT]), as well as primers specific for several endogenous retroviruses[30] in duplicate. The delta cycle threshold (dCT) value was calculated by subtracting the average value obtained for GAPDH from the experimental value.

Analysis of A-to-G editing

RNA from two kidneys isolated 18 h after intravenous injection of pentostatin and from two kidneys from untreated mice were sequenced by next generation sequencing (NGS) (GATC Biotech, Germany), and reads were trimmed, aligned, and analyzed (Genevia, Finland). A-to-I editing, observable in RNA sequencing (RNA-seq) data as A-to-G and T-to-C base substitutions for forward- and reverse-transcribed genes, was studied at genomic sites listed in the RADAR ("A Rigorously Annotated Database of A-to-I RNA Editing") database.[31] Duplicate reads were removed, and unique reads were counted with SAMtools, version 1.3.[32,33] The SAMtools mpileup function, with a parameter -q10 and a mapping quality threshold of 10 on the Phred scale, was used to count reads with a reference base or an edited base at genomic sites listed in RADAR. All sites with less than 5 aligned reads passing the quality threshold were discarded from downstream analyses and visualizations. The fraction of the reads supporting an editing event listed in RADAR was interpreted as the editing frequency.

Drugs

Pentostatin (Sigma), stored as powder at −20, was diluted in PBS for a working concentration of 10 mg/mL and used immediately.

Tumor models and treatment

Mice were inoculated subcutaneously with 1×10^6 tumor cells in 200 μL PBS. Tumor sizes were measured with a caliper every second day for calculating tumor volumes using the equation $(a^2 \times b)/2$ (where a is width; b is length). Animals were sacrificed when exhibiting signs of impaired health or when tumor volume exceeded 1 cm^3. Pentostatin (Sigma) was injected intravenously when tumors were palpable (day 6 for MB49 and day 7 for CT26/NY-ESO-1). When indicated, 1 mg of anti-IFNAR1 blocking antibody (MAR1-5A3; Bio X Cell) solution was injected intraperitoneally at the same day as pentostatin. When indicated, 100 μg of anti-PD1-blocking antibody (BioLegend; RMP1−14) solution was injected intravenous.

Bioluminescent *in vivo* imaging

Bioluminescence *in vivo* imaging of tumor-bearing IFN-β reporter mice was performed on IVIS Lumina (PerkinElmer) at specific time points post-pentostatin injection. D-luciferin (Synchem), dissolved in PBS (15 mg/mL stock) and sterile filtered, was injected (150 μg/g intraperitoneally). Emitted photons from live animals were quantified 10−20 min post-luciferin injections with an exposure time of 3 min. Regions of interest (ROIs) were quantified for average radiance (photons s^{-1} cm^{-2} sr^{-1}; IVIS Living Image 4.0).

Immunofluorescence staining

$CD8^+$ staining was performed on 6−8 μm sections of cryo-preserved tumors. Cryosections were fixed for 5 min in −20 cold methanol and equilibrated for 5 min in PBS. After three washes in PBS containing 0.1% Tween 20 (PBST), slides were blocked for 1 h at RT in 12%

BSA in PBS containing 0.1% "NP-40" (blocking buffer). CD8 antibody (eBioscience, Thermo Fisher Scientific), phycoerythrin (PE) conjugated at 1:1,000 dilution in blocking buffer, was incubated overnight at 4°. Sections were washed three times in PBST. Nuclei were stained with IUPAC-Bezeichnung: 4',6-Diamidino-2-phenylindol (DAPI) (Sigma; 1:2,000). After three washes with PBST, sections were quickly washed in water, mounted in fluorescent mounting medium, and air dried for 2 h at RT. Immunofluorescence images were acquired using a Zen Pro Axio Zeiss microscope and software.

Cell survival assay

Cell lines were seeded (5,000 cells per well) in 300 μL of complete medium in a 48-well plate. 1 day later, supernatants were replaced by 200 μL of complete medium. Different doses of pentostatin were added in 200 μL. After 3 days of growth, wells were washed gently with minimum essential medium eagle (MEM) and frozen at −80°C in 500 μL of PBS. The next day, plates were placed at RT for more than 3 h and spun for 5 min at 1,500 rpm. Supernatants (10 μL) were transferred in a 96-well plate with addition of 40 μL substrate for lactate dehydrogenase (LDH) from the Cytotox96 Kit (Promega). Reactions were stopped with the addition of 40 μL stop solution, and plates were measured at OD 490 (OD_{490}). Background was the value of 10 μL PBS + 40 μL substrate + 40 μL stop solution. The percentage of surviving cells was calculated according to the following formula: (experimental value − background)/(untreated cells − background) × 100.

Statistical analyses and data presentation

All results are expressed as mean ± SD. Unpaired two-tailed Student's t test was used for comparison of two groups. One-way analysis of variance (ANOVA) was performed when more than two groups were compared and when determined significant ($p < 0.05$).

SUPPLEMENTAL INFORMATION

Supplemental information can be found online at https://doi.org/10.1016/j.ymthe.2021.09.022.

ACKNOWLEDGMENTS

We thank Dr. Stefan Linenklaus for giving us the reporter mouse that contains the firefly luciferase gene in place of the IFN-β-coding region and Professor Pal Johansen for the help in obtaining KO mice. This work was supported by the Swiss National Science Foundation (31003A_140901, Switzerland), University Research Priority Project (URPP) "Translational Cancer Research" (University of Zurich, Switzerland) Helmut Horten Stiftung (Switzerland), Monique Dornonville de la Cour Stiftung (Switzerland), and the "MERIT" project supported by the FP7 European Union's Research and Innovation Funding Programme.

AUTHOR CONTRIBUTIONS

Acquisition, analysis, and interpretation of data and drafted the work, M.T.; conception and support of the work and substantively revised the manuscript, T.M.K.; conception and design of the work; acquisition, analysis, and interpretation of data; and drafted the work, S.P.

DECLARATION OF INTERESTS

The authors declare no competing interests.

REFERENCES

1. Agarwal, R.P., Spector, T., and Parks, R.E., Jr. (1977). Tight-binding inhibitors–IV. Inhibition of adenosine deaminases by various inhibitors. Biochem. Pharmacol. *26*, 359–367.
2. Wilson, P.K., Szabados, E., Mulligan, S.P., and Christopherson, R.I. (1998). Comparative effects of cladribine, fludarabine and pentostatin on nucleotide metabolism in T- and B-cell lines. Int. J. Biochem. Cell Biol. *30*, 833–842.
3. Cass, C.E., and Au-Yeung, T.H. (1976). Enhancement of 9-beta-d-arabinofuranosyladenine cytotoxicity to mouse leukemia L1210 in vitro by 2′-deoxycoformycin. Cancer Res. *36*, 1486–1491.
4. Caron, N., Lee, S.H., and Kimball, A.P. (1977). Effects of 2′-deoxycoformycin, 9-beta-D-arabinofuranosyladenine 5′-phosphate, and 1-beta-D-arabinofuranosylcytosine triple combination therapy on intracerebral leukemia 1210. Cancer Res. *37*, 3274–3279.
5. Dillman, R.O., Yu, A.L., and Qiao, C.N. (1988). Repeated pentostatin (2'deoxycoformycin)-induced remissions in a patient with advanced chronic lymphocytic leukemia. West. J. Med. *148*, 334–337.
6. Döhner, H., Ho, A.D., Thaler, J., Stryckmans, P., Sonneveld, P., de Witte, T., Lechner, K., Lauria, F., Bödewadt-Radzun, S., Suciu, S., et al. (1993). Pentostatin in prolymphocytic leukemia: phase II trial of the European Organization for Research and Treatment of Cancer Leukemia Cooperative Study Group. J. Natl. Cancer Inst. *85*, 658–662.
7. Braiteh, F., Ng, C., and Kurzrock, R. (2006). Refractory Hodgkin lymphoma responds to pentostatin (2'-deoxycoformycin). Leuk. Lymphoma *47*, 373–375.
8. Grever, M.R., Bisaccia, E., Scarborough, D.A., Metz, E.N., and Neidhart, J.A. (1983). An investigation of 2′-deoxycoformycin in the treatment of cutaneous T-cell lymphoma. Blood *61*, 279–282.
9. Kurzrock, R., Pilat, S., and Duvic, M. (1999). Pentostatin therapy of T-cell lymphomas with cutaneous manifestations. J. Clin. Oncol. *17*, 3117–3121.
10. Grever, M.R., Siaw, M.F., Jacob, W.F., Neidhart, J.A., Miser, J.S., Coleman, M.S., Hutton, J.J., and Balcerzak, S.P. (1981). The biochemical and clinical consequences of 2′-deoxycoformycin in refractory lymphoproliferative malignancy. Blood *57*, 406–417.
11. Spiers, A.S., Parekh, S.J., and Bishop, M.B. (1984). Hairy-cell leukemia: induction of complete remission with pentostatin (2′-deoxycoformycin). J. Clin. Oncol. *2*, 1336–1342.
12. Kraut, E.H., Bouroncle, B.A., and Grever, M.R. (1986). Low-dose deoxycoformycin in the treatment of hairy cell leukemia. Blood *68*, 1119–1122.
13. Grever, M., Kopecky, K., Foucar, M.K., Head, D., Bennett, J.M., Hutchison, R.E., Corbett, W.E., Cassileth, P.A., Habermann, T., Golomb, H., et al. (1995). Randomized comparison of pentostatin versus interferon alfa-2a in previously untreated patients with hairy cell leukemia: an intergroup study. J. Clin. Oncol. *13*, 974–982.
14. Begleiter, A., Glazer, R.I., Israels, L.G., Pugh, L., and Johnston, J.B. (1987). Induction of DNA strand breaks in chronic lymphocytic leukemia following treatment with 2′-deoxycoformycin in vivo and in vitro. Cancer Res. *47*, 2498–2503.
15. Johnston, J.M., and Kredich, N.M. (1979). Inhibition of methylation by adenosine in adenosine deaminase-inhibited, phytohemagglutinin-stimulated human lymphocytes. J. Immunol. *123*, 97–103.
16. Kredich, N.M. (1980). Inhibition of nucleic acid methylation by cordycepin. In vivo synthesis of S-3′-DEOXYADENOSYLMETHIONINE BY WI-L2 human lymphoblasts. J. Biol. Chem. *255*, 7380–7385.
17. Glazer, R.I., and Hartman, K.D. (1980). Evidence that the inhibitory effect of adenosine, but not cordycepin, on the methylation of nuclear RNA is mediated by S-adenosylhomocysteine hydrolase. Mol. Pharmacol. *18*, 483–490.
18. Hershfield, M.S., Kredich, N.M., Koller, C.A., Mitchell, B.S., Kurtzberg, J., Kinney, T.R., and Falletta, J.M. (1983). S-adenosylhomocysteine catabolism and basis for acquired resistance during treatment of T-cell acute lymphoblastic leukemia with 2′-

deoxycoformycin alone and in combination with 9-beta-D-arabinofuranosyladenine. Cancer Res. *43*, 3451–3458.

19. Karikó, K., Buckstein, M., Ni, H., and Weissman, D. (2005). Suppression of RNA recognition by Toll-like receptors: the impact of nucleoside modification and the evolutionary origin of RNA. Immunity *23*, 165–175.

20. Devarkar, S.C., Wang, C., Miller, M.T., Ramanathan, A., Jiang, F., Khan, A.G., Patel, S.S., and Marcotrigiano, J. (2016). Structural basis for m7G recognition and 2′-O-methyl discrimination in capped RNAs by the innate immune receptor RIG-I. Proc. Natl. Acad. Sci. USA *113*, 596–601.

21. Züst, R., Cervantes-Barragan, L., Habjan, M., Maier, R., Neuman, B.W., Ziebuhr, J., Szretter, K.J., Baker, S.C., Barchet, W., Diamond, M.S., et al. (2011). Ribose 2′-O-methylation provides a molecular signature for the distinction of self and non-self mRNA dependent on the RNA sensor Mda5. Nat. Immunol. *12*, 137–143.

22. Freund, I., Eigenbrod, T., Helm, M., and Dalpke, A.H. (2019). RNA Modifications Modulate Activation of Innate Toll-Like Receptors. Genes (Basel) *10*, E92.

23. Rettig, L., Haen, S.P., Bittermann, A.G., von Boehmer, L., Curioni, A., Krämer, S.D., Knuth, A., and Pascolo, S. (2010). Particle size and activation threshold: a new dimension of danger signaling. Blood *115*, 4533–4541.

24. Tusup, M., and Pascolo, S. (2017). Generation of Immunostimulating 130 nm Protamine-RNA nanoparticles. Methods Mol. Biol. *1499*, 155–163.

25. Grosso, J.F., and Jure-Kunkel, M.N. (2013). CTLA-4 blockade in tumor models: an overview of preclinical and translational research. Cancer Immun. *13*, 5.

26. Lienenklaus, S., Cornitescu, M., Zietara, N., Łyszkiewicz, M., Gekara, N., Jabłónska, J., Edenhofer, F., Rajewsky, K., Bruder, D., Hafner, M., et al. (2009). Novel reporter mouse reveals constitutive and inflammatory expression of IFN-beta in vivo. J. Immunol. *183*, 3229–3236.

27. Meixlsperger, S., Leung, C.S., Rämer, P.C., Pack, M., Vanoaica, L.D., Breton, G., Pascolo, S., Salazar, A.M., Dzionek, A., Schmitz, J., et al. (2013). CD141+ dendritic cells produce prominent amounts of IFN-α after dsRNA recognition and can be targeted via DEC-205 in humanized mice. Blood *121*, 5034–5044.

28. Lang, K.S., Recher, M., Junt, T., Navarini, A.A., Harris, N.L., Freigang, S., Odermatt, B., Conrad, C., Ittner, L.M., Bauer, S., et al. (2005). Toll-like receptor engagement converts T-cell autoreactivity into overt autoimmune disease. Nat. Med. *11*, 138–145.

29. Muraoka, D., Kato, T., Wang, L., Maeda, Y., Noguchi, T., Harada, N., Takeda, K., Yagita, H., Guillaume, P., Luescher, I., et al. Peptide vaccine induces enhanced tumor growth associated with apoptosis induction in CD8+ T cells. J. Immunol. 185, 3768−3776.

30. Chiappinelli, K.B., Strissel, P.L., Desrichard, A., Li, H., Henke, C., Akman, B., Hein, A., Rote, N.S., Cope, L.M., Snyder, A., et al. (2015). Inhibiting DNA Methylation Causes an Interferon Response in Cancer via dsRNA Including Endogenous Retroviruses. Cell *162*, 974–986.

31. Ramaswami, G., and Li, J.B. (2014). RADAR: a rigorously annotated database of A-to-I RNA editing. Nucleic Acids Res. *42*, D109–D113.

32. Li, H., and Durbin, R. (2009). Fast and accurate short read alignment with Burrows-Wheeler transform. Bioinformatics *25*, 1754–1760.

33. Li, H., Handsaker, B., Wysoker, A., Fennell, T., Ruan, J., Homer, N., Marth, G., Abecasis, G., and Durbin, R.; 1000 Genome Project Data Processing Subgroup (2009). The Sequence Alignment/Map format and SAMtools. Bioinformatics *25*, 2078–2079.